ESTIMATION OF RESERVES WITH UNKNOWN SPILLPOINT

PETTER ABRAHAMSEN, RAGNAR HAUGE, AND KNUT HEGGLAND
NORWEGIAN COMPUTING CENTER

September 1996

1. Introduction

Consider a potential oil filled trap identified on a seismic travel time map. The maximum possible gross rock volume is determined by the shape of the cap rock and the spillpoint. We will outline a method for assessing this volume and moreover, investigate the uncertainty in this volume.

By generating a set of possible cap rocks the spillpoint for each cap rock can be detected and the volume within the trap can be calculated. Finally a histogram of the volumes can inspected for upside and downside potential and the economical risk of the prospect can be evaluated.

2. Depth conversion of cap rock

Consider the potential trap in the travel time map in Figure 1. A velocity model must be established to locate the depth to the subsurface. A velocity model of the form $v = v_0 + k \cdot t$ has been used, where v_0 is a partially known constant velocity, and k is a partially known constant multiplied by the travel time, t. The second term

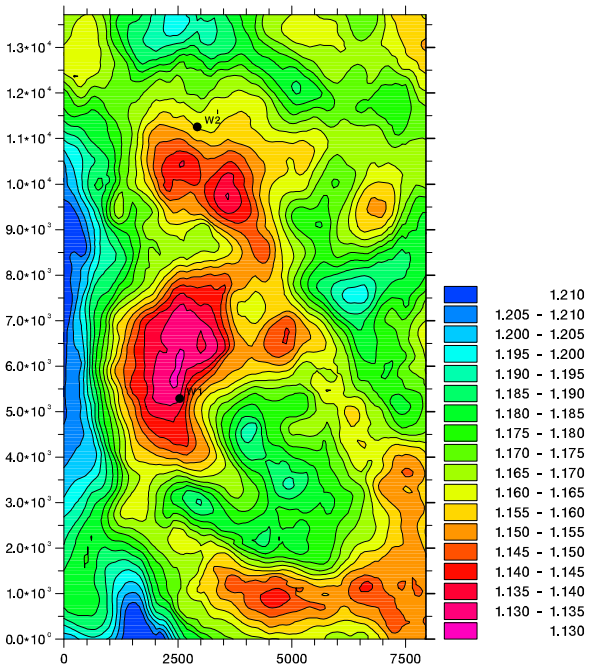

Figure 1. Travel time to cap rock in one way seconds. The size of the area is approximately 7.5km × 14km.

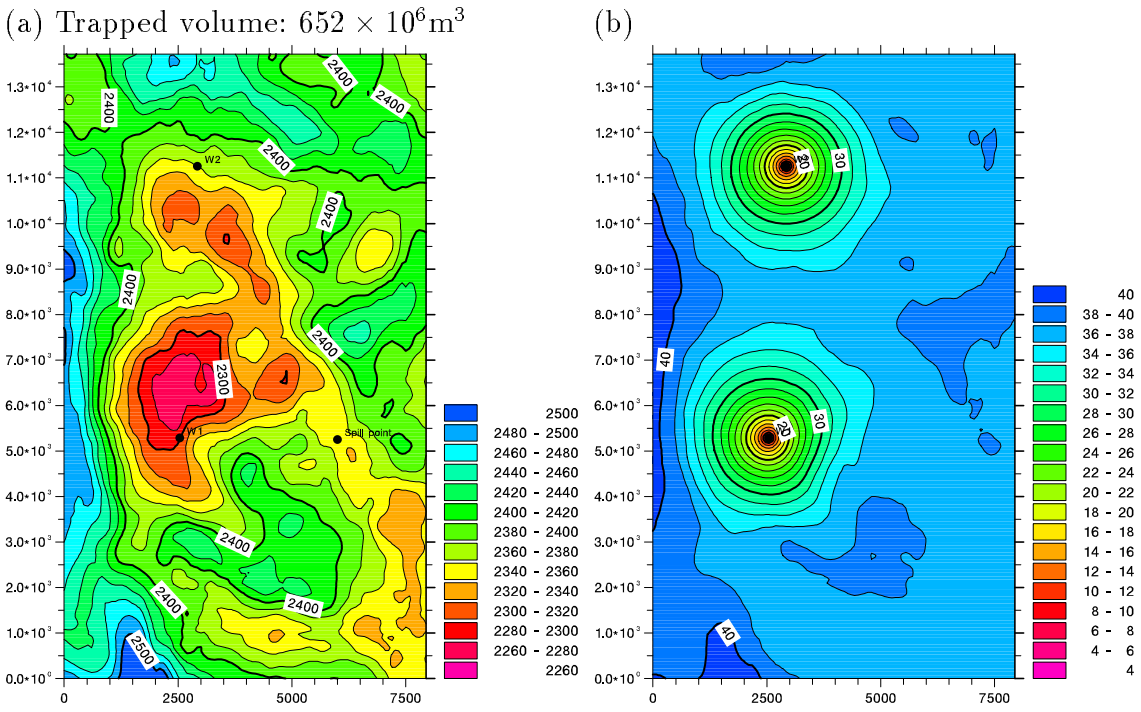

FIGURE 2. Predicted depth in meter (a) with corresponding prediction error (b).

will, for positive k's give an increase in velocity for increasing time (depth). Depth observations in the two wells in FIGURE 1 are used to improve the precision on the partially unknown parameters, v_0 and k.

The uncertainty in the depth to the contact is caused by uncertainty in travel time interpretations and uncertainty in the velocity model. The uncertainty in the travel times are assumed to account for approximately $\pm$15m (standard deviation)[1] in the depth of the cap rock. The uncertainty in the velocities is caused by two factors. The two parameters v_0 and k are not known and can only be accurately estimated from data when a large number well observations are available. Furthermore, if these two parameters where accurately known there would still be local velocity anomalies which is not accounted for by the linear velocity model. The local velocity anomalies are assumed to be approximately $\pm$25m/s (standard deviation).

To integrate the data a geostatistical method called Bayesian kriging (Kitanidis 1986, Omre 1987, Abrahamsen, Omre & Lia 1991, Abrahamsen 1993) has been used. The basic idea is to let the well data improve a prior guess on v_0 and k to find a velocity trend. Then, the depth to the subsurface is locally adjusted to match the well observations. The result is seen in FIGURE 2. The velocity field can also be predicted in the same way leading to the maps in FIGURE 3. Note that Bayesian kriging supplies a map of the local prediction error.

The travel time uncertainty and the velocity anomalies are assumed to be laterally continuous. To model this continuity a spherical variogram (Journel & Huijbregts

[1] This amounts to approximately $\pm$15msec. two way travel time standard error.

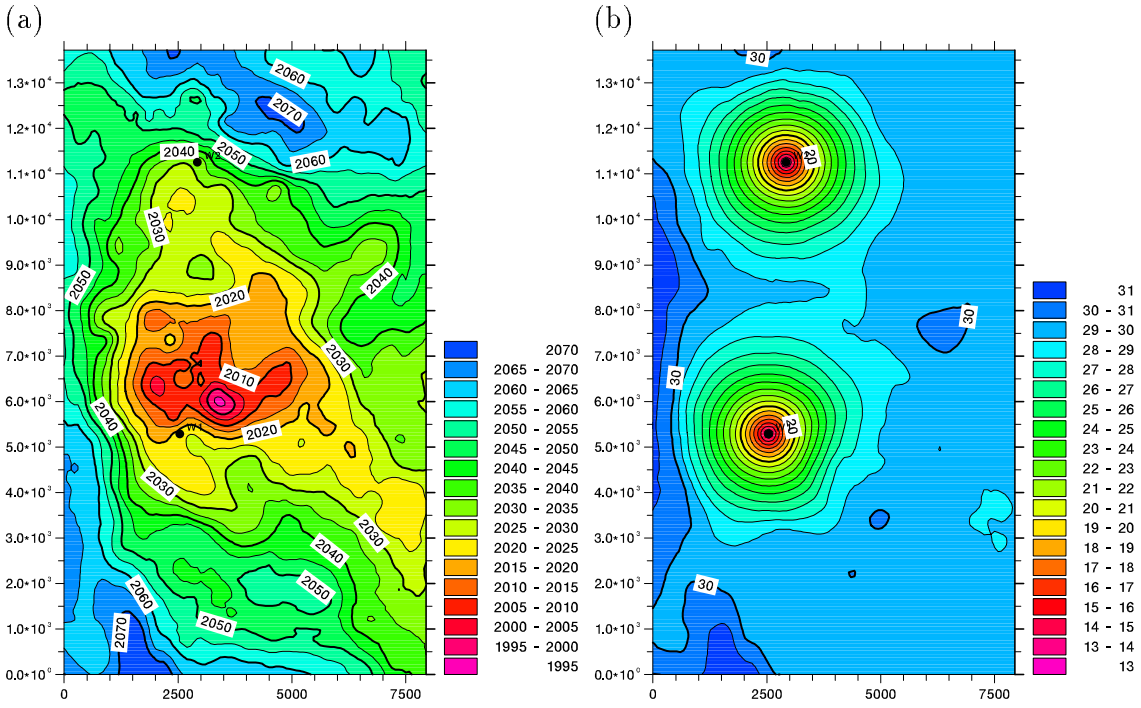

FIGURE 3. Predicted velocity in meter/second (a) with corresponding prediction error (b).

1978) with correlation range 3000m has been used for both. This variogram has proved reasonable on Statfjord data.

An important property of Bayesian kriging is that it works in the exploration phase with few and even no wells. With no well observations the prior guess on v_0 and k are left unchanged and the uncertainty in these parameters might make the final depth predictions very uncertain.

Instead of predicting 'the most probable' depth map, it is possible to generate possible depth maps using conditional simulation. There is a strong relationship between prediction and conditional simulation. The average of a large set of simulated maps will be very close to the predicted map. Four different simulated realizations are found in FIGURE 4.

3. SPILLPOINT DETECTION

A spillpoint is not uniquely defined unless a point within the trap has been located. In the example the location of well 'W1' has been chosen as this point. The uppermost value in the depth prediction map could also be a candidate. Moreover, a certain area containing the spillpoint must be identified. Typically this is the rectangular area of the map which was chosen in this example. It is necessary to restrict the spillpoint to an area since the considered trap could be a local trap within a much larger trap.

In FIGURE 2(a) the spillpoint is marked by a small black disc in the 'yellow channel' leading out of the area to the right. In the simulated realizations FIGURE 4(a-c) the

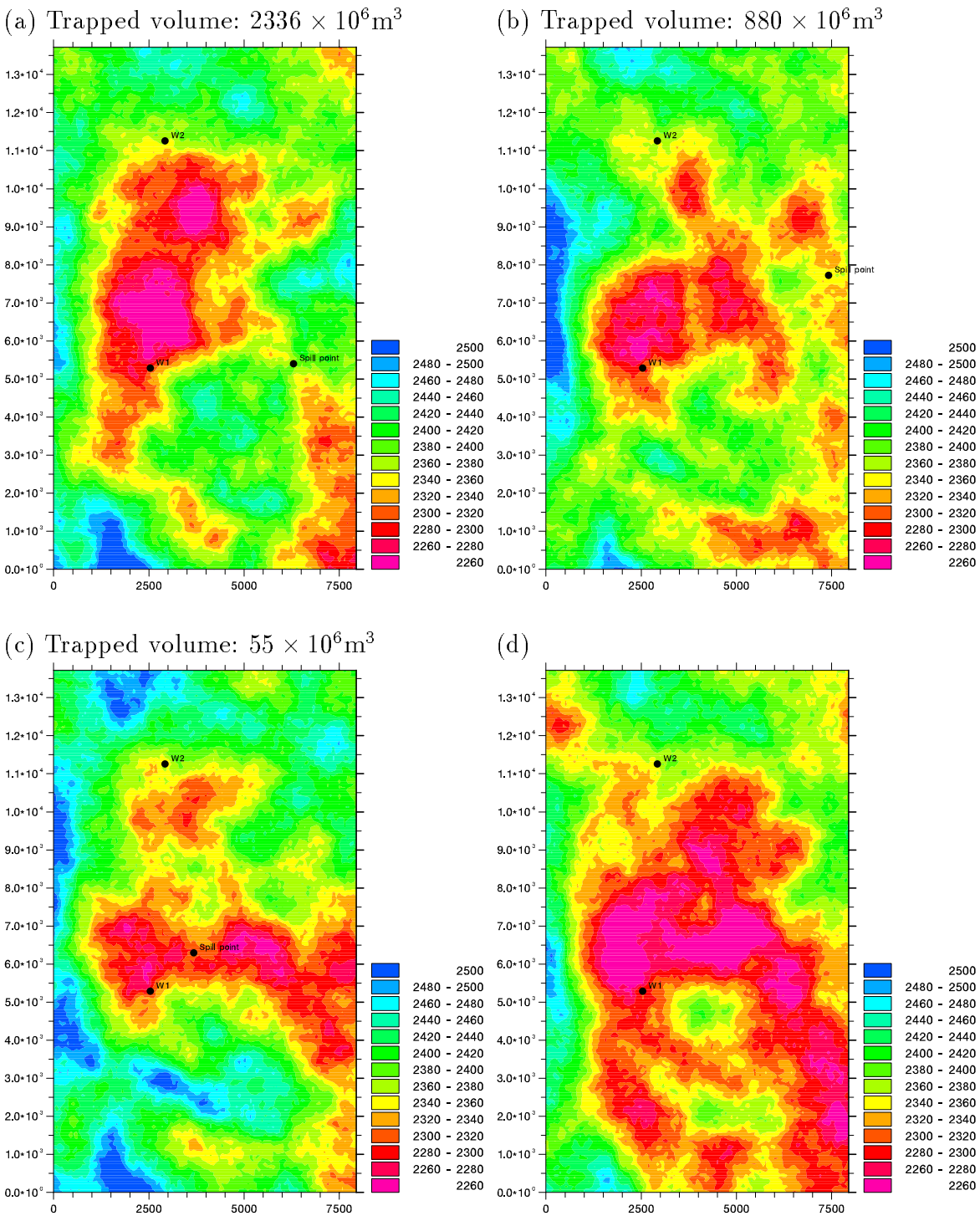

FIGURE 4. Simulated depth. Realization with maximum volume (a), median volume (b), and minimum volume (c). In (d) no spillpoint below the depth to well 'W1' could be found.

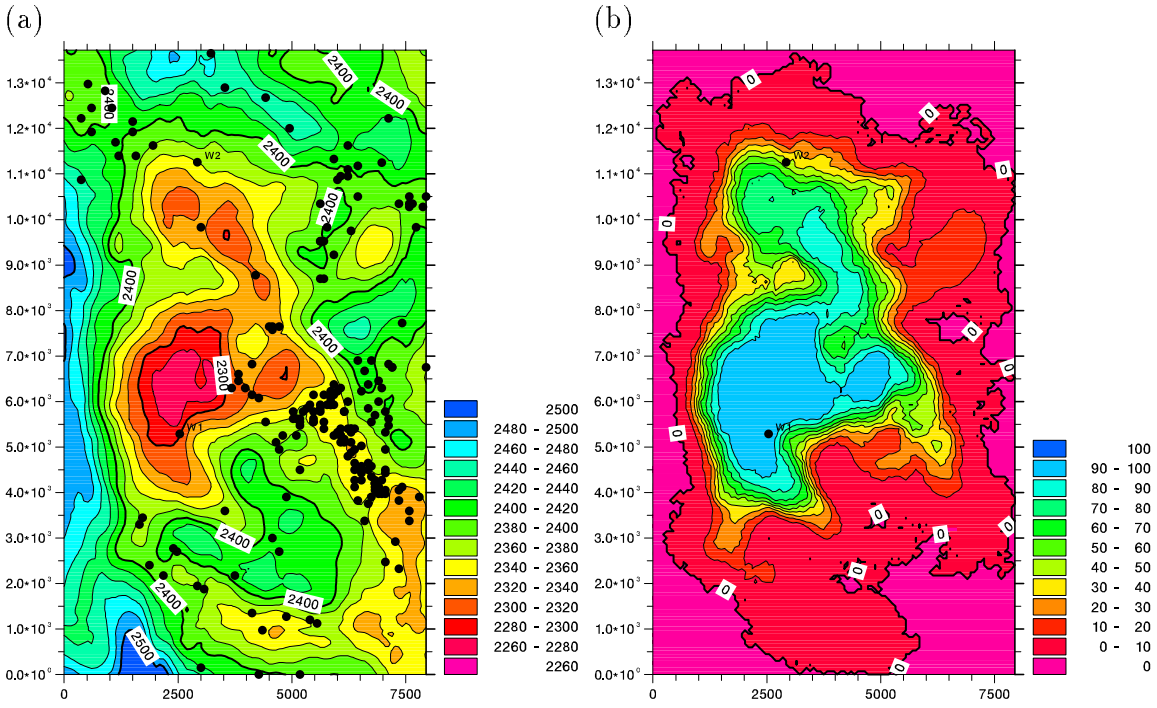

FIGURE 5. Spillpoints (black dots) plotted on map of predicted depth (a). In (b) the probability for a point being within the trap is plotted.

spillpoints are marked similarly. We see that the location of the spillpoints vary a lot. Finally in FIGURE 4(d) no spillpoint was found deeper than well 'W1'. This is a problem in approximately 1.5% of the realizations in this case. If the uppermost location in FIGURE 2(a) was chosen as the point within the trap, this situation would probably never occur.

In FIGURE 5(a) spillpoints from 197 simulated realizations (3 realizations had no spillpoint) are marked on the predicted depth map. We see a large variation in locations but the major number of the spillpoints are located at the 'yellow channel' leading out of the area to the right. FIGURE 5(b) gives the probability for a point being within the trap. It is seen that traps can be found within large areas. However, the area above well 'W1' is by far the most probable area belonging to the trap.

4. VOLUMES

FIGURE 6(a) shows a probability density plot (smoothed histogram) for trapped volumes from 197 simulated realizations. The mean and median of the trapped volumes are $965 \times 10^6 \mathrm{m}^3$ and $880 \times 10^6 \mathrm{m}^3$ respectively. Thus the volume for the prediction ($652 \times 10^6 \mathrm{m}^3$) is pessimistic. There is a possible downside for almost no volume but the upside is encouragingly large.

The probability density plot for depth to the spillpoint is found in FIGURE 6(b).

FIGURE 7(a) shows a map of the mean column for the simulated realizations with the corresponding standard deviations in FIGURE 7(b). Note that the standard deviations do not approach zero at well locations since the spillpoint is uncertain.

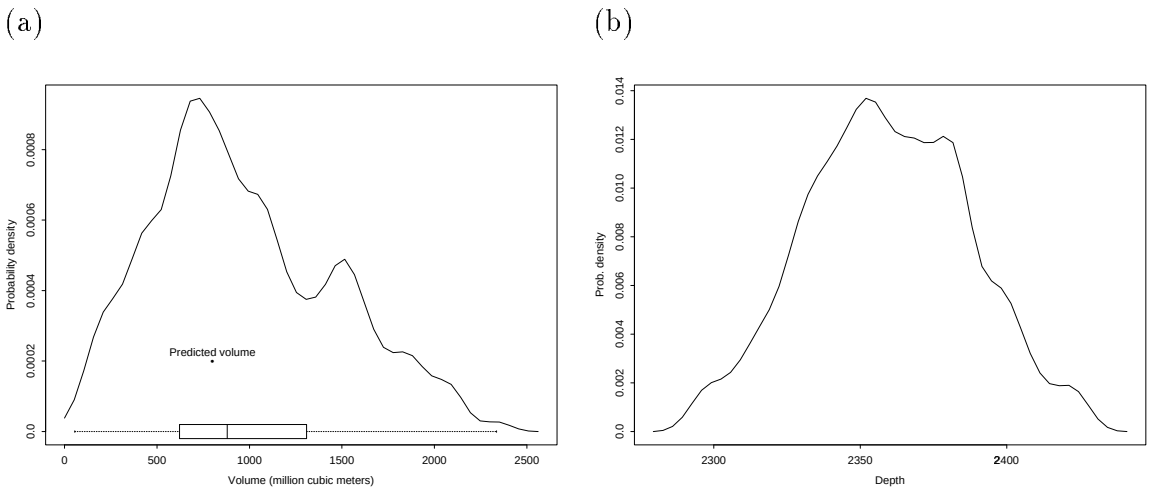

FIGURE 6. Probability distributions (histograms) for volume within trap (a), and depth to spillpoint (b). The volume for the predicted surface is $652 \times 10^6 \mathrm{m}^3$ with spill point at 2353m. The box plot at the bottom of (a) marks the extremes, the quartiles, and the median. The expectation (mean) of the trapped volume is $965 \times 10^6 \mathrm{m}^3$.

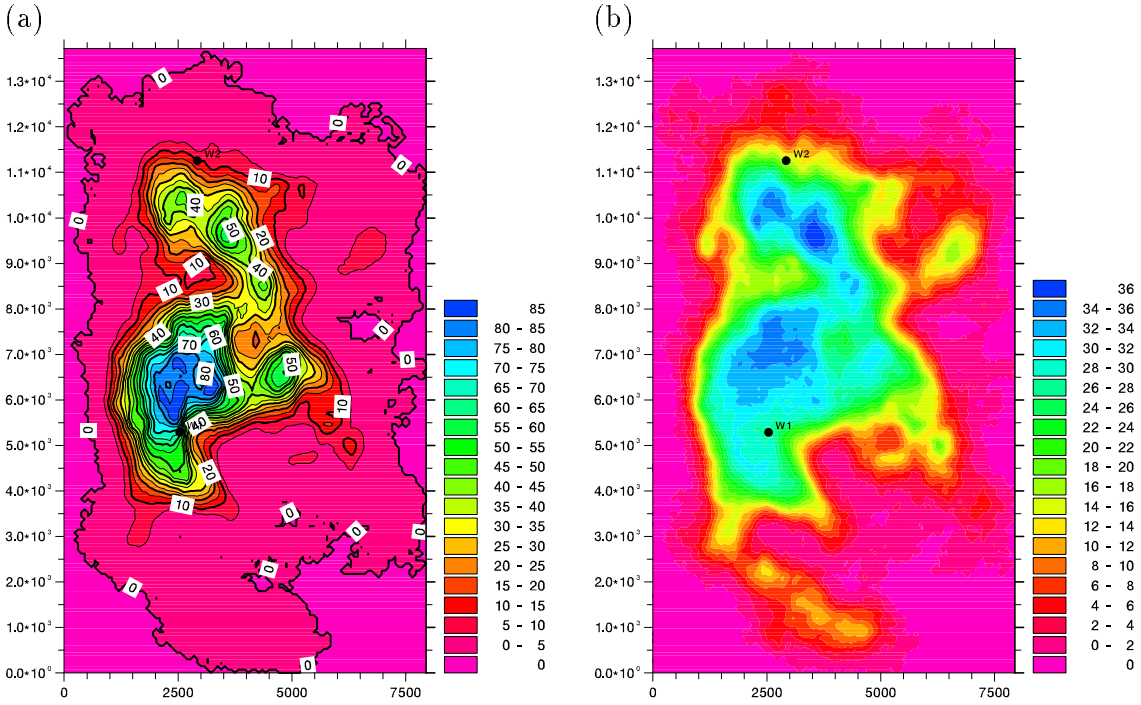

FIGURE 7. The average column for all simulated realizations (a), and the corresponding standard deviation (b).

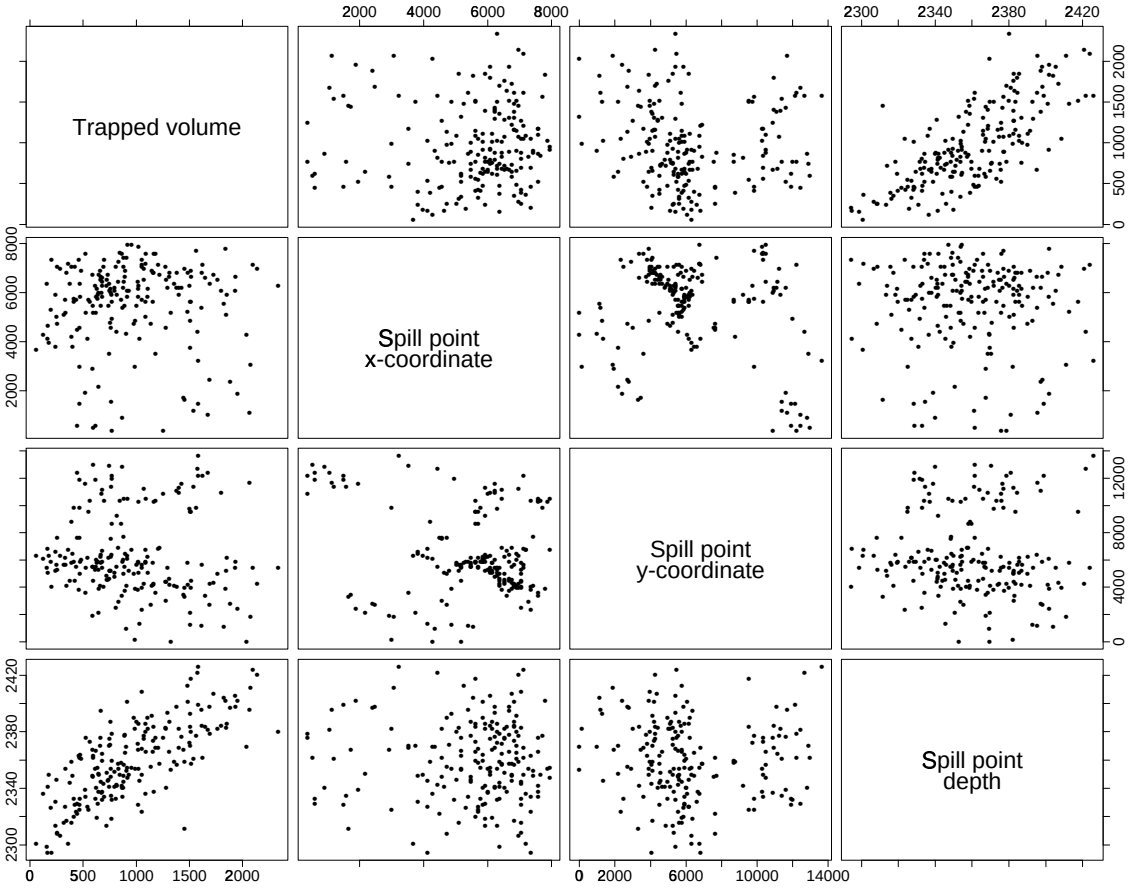

FIGURE 8. Scatter plots of trapped volume, x-coordinate, y-coordinate, and depth at spillpoint.

FIGURE 8 shows scatter plots of pairwise combinations of trapped volume, x-coordinate, y-coordinate, and depth at spillpoint. As expected, there is a strong relationship between volume and depth at the spillpoint. A more subtle observations is that the shallow spillpoints and the smallest volumes are associated with y-coordinates close to 6000m. These are the spillpoints close to the red area in FIGURE 5(a). Finally we see a trend towards larger volumes as the spillpoint is located either in the far north or far south. There are no apparent relationships to the x-coordinate except from the patterns seen when plotting them with the y-coordinates.

5. CLOSING REMARKS

An approach for estimating the volume within a potential trap has been demonstrated. The major result is a map of possible spillpoints in FIGURE 5(a), and probability distributions (histograms) for volumes in FIGURE 6. The map of spillpoints shows more possibilities than what would be expected from a quick look at the travel time map in FIGURE 1.

The calculated trapped volumes give the upside potential of the trap. Whether the trap is completely filled or not depends on other factors such as relative position

to and volume of source rocks.

In this particular case the 'predicted volume' (calculated from the predicted subsurface) are in reasonable agreement with the median of the simulated volumes. A measure of the downside and upside potentials however, are impossible to evaluate from a prediction. To obtain an understanding of the true potential of the trap simulation studies must be performed.

In this particular case the upside potential is leading to a mean value of the simulated volumes significantly higher than the predicted volume. High volumes in this particular case are partly caused by the closure of the 'yellow channel' leading out to the right in FIGURE 5(a). In cases where the spillpoints are more uniformly positioned around a dome, the simulated volumes will probably be smaller than the 'predicted volume' since there is a large probability for a flank being shallower than the predicted depth values.

5.1. Comments on speed. Spillpoint detection and subsurface simulation are the two main tasks for obtaining the results. The grid used in the example is an ASCII formated `IRAP` grid with $107 \times 184 \approx 20.000$ grid nodes. HORIZON (Abrahamsen & Omre 1992) was used for simulating the subsurfaces and used 3.8 CPU seconds for each realization on a `SUN Ultrasparc` workstation. The spillpoint detection takes 0.8 CPU seconds for each realization. Generating average grids and other external data manipulation on `IRAP` grids used approximately two thirds of the overall run time in the simulation loop. Using binary grids would reduce the total amount of time dramatically. Thus, computational speed is a minor problem and several hundred realizations can be generated within an hour. In the current example 200 realizations were considered and this should be sufficient in all practical applications.

REFERENCES

Abrahamsen, P. (1993), Bayesian kriging for seismic depth conversion of a multi-layer reservoir, *in* A. Soares, ed., 'Geostatistics Tróia '92', proc. '4th Inter. Geostat. Congr.', Tróia Portugal, 1992, Kluwer Academic Publishers, Dordrecht, pp. 385–398.

Abrahamsen, P. & Omre, H. (1992), Horizon 4.0 — geometrical module, user guide and theory, NR-note SAND/01/1992, Norwegian Computing Center, P.O.Box 114 Blindern, N-0314 Oslo, Norway, 112 pp.
(revised 1994).

Abrahamsen, P., Omre, H. & Lia, O. (1991), 'Stochastic models for seismic depth conversion of geological horizons', SPE 23138. Presented at Offshore Europe, Aberdeen, 329–341 pp.

Journel, A. G. & Huijbregts, C. J. (1978), *Mining Geostatistics*, Academic Press Inc., London, 600 pp.

Kitanidis, P. K. (1986), 'Parameter uncertainty in estimation of spatial functions: Bayesian analysis', *Water Resour. Res.* **22**(4), 499–507.

Omre, H. (1987), 'Bayesian kriging—merging observations and qualified guesses in kriging', *Math. Geol.* **19**(1), 25–39.